Original Article	*Curr. Appl. Sci.*, **2024**, *2*(2):119-134 DOI: 10.22034/cas.2024.476900.1042	Current Applied Sciences

Comprehensive Analysis of Impedance Spectroscopy and Conductivity Evaluation of Ionic Transport in Lithium Borate Glasses

Mohammad Reza Shoar Abouzari

Department of Physics, University of Zabol, Zabol, Iran

Corresponding author's e-mail: *abouzari@uoz.ac.ir*

Article Information

Received: 04 September 2024
Revised: 15 September 2024
Accepted: 17 September 2024
Published online: 27 November 2024

Keywords

Ion conductivity
Impedance spectroscopy
Impedance semicircle
Constant phase element

Abstract

This paper presents a comprehensive investigation of the electrical properties of ionic conductors, with a particular focus on lithium borate glasses, using impedance spectroscopy. We explore the complex behavior of these materials across a wide frequency range, examining both bulk samples and thin films to elucidate the fundamental mechanisms of ionic conduction and interfacial phenomena. To address the limitations of conventional equivalent circuit models, we use the Constant Phase Element (CPE) as a more accurate alternative to simple RC (resistor-capacitor) circuits for describing non-ideal behavior in real systems. We provide a thorough derivation and validation of a new relationship between CPE parameters and conventional capacitance values, offering improved tools for interpreting impedance data. The paper also addresses practical challenges in impedance spectroscopy measurements, including frequency range limitations and their impact on data interpretation. We propose methods for overcoming these challenges and extracting meaningful information from partial impedance spectra. Furthermore, we explore the physical origins of the observed non-ideal behavior, discussing various models, such as the jump relaxation model, and relating them to the microstructure and composition of the ionic conductors. This work provides crucial insights into ion transport mechanisms in glassy electrolytes, offers practical guidelines for analyzing impedance spectroscopy data, and has significant implications for the development of ionic conductors in applications such as solid-state batteries and sensors. This work lays the foundation for future research on a broader range of compositions and structures, as well as the development of more sophisticated models for ionic conducting systems.

1. Introduction

Impedance spectroscopy has emerged as a powerful and versatile technique for characterizing the electrical properties of materials, particularly in the field of ionic conductivity. This non-destructive method provides valuable insights into the complex interplay of charge transport mechanisms within ionic conductors, making it an indispensable tool for researchers and engineers alike.

Ionic conductivity, the measure of a material's ability to conduct ions, plays a crucial role in numerous applications, ranging from solid-state batteries [1, 2] and fuel cells to sensors and electrochemical devices [3]. As the demand for high-performance energy storage and conversion systems continues to grow, understanding and optimizing ionic conductivity has become increasingly important [4].

Impedance spectroscopy is a powerful analytical technique that measures the complex impedance of a sample as a function of frequency [5]. This well-established method allows for the determination of various electrical properties, including conductivity, capacitance, and dielectric constant. Unlike direct current (DC) methods, impedance spectroscopy can be employed even with blocking electrodes, making it versatile for a wide range of materials and systems [6].

In most electrical systems, the measured impedance is influenced by multiple variables. By strategically selecting different frequency ranges, researchers can probe and characterize a diverse array of material properties [7]. This flexibility makes impedance spectroscopy an invaluable tool in fields such as materials science, electrochemistry, and solid-state physics [8].

Impedance spectroscopy provides not only specific physical properties of samples, such as their conductivity, but also information about the geometric structure of the investigated material. This information is obtained by defining an appropriate equivalent circuit to describe the measured data [7]. The equivalent circuit must be constructed in such a way that its impedance spectrum accurately represents the measured data.

This paper aims to provide a comprehensive overview of impedance spectroscopy as applied to the study of ionic conductivity. We will discuss the fundamental principles underlying this technique, explore various experimental setups and data analysis methods, and examine case studies that demonstrate its effectiveness in characterizing lithium borate ionic conductivity.

2. Materials and Methods

In this section, we delve into the method of impedance spectroscopy. We will conduct complex impedance analysis for RC circuits and examine impedance semicircles. Furthermore, we will theoretically investigate compressed impedance semicircles, which are commonly observed in experimental ionic conductivity results, using the constant phase element model.

2.1 *Analysis of the conductivity spectra*

Impedance of an electrical element is defined as a function of frequency by the equation

$$Z(\omega) = \frac{V(\omega)}{I(\omega)}, \tag{2.1}$$

where I(ω) is the electrical response (current) of the element on the applied potential V(ω). Considering the possible phase shift between I(ω) and V(ω), the impedance is expressed as a complex quantity

$$\hat{Z}(\omega) = \left|Z(\omega)\right| \cdot e^{i\theta} \tag{2.2}$$

$$\hat{Z}(\omega) = Z'(\omega) + iZ''(\omega). \tag{2.3}$$

Here, the symbol $\hat{Z}$ is used for complex impedance. Z'(ω) and Z"(ω) are the real and imaginary part of the impedance, and θ is the phase difference between the electrical potential and current. Instead of using impedance directly, the dynamic behavior of ions is often characterized by the specific conductivity, which is independent of the sample's geometric properties. The specific conductivity can be expressed in terms of the measured impedance for a sample with thickness d and surface area S as

$$\hat{\sigma}(\omega) = \frac{d}{\hat{Z}(\omega) \cdot S}. \qquad (2.4)$$

Equations (2.3) and (2.4) yield the following statements for the real and imaginary part of specific conductivity

$$\hat{\sigma}(\omega) = \sigma'(\omega) + i\sigma''(\omega)$$

$$\sigma'(\omega) = \frac{d}{S} \cdot \frac{Z'}{|\hat{Z}|^2} \quad ; \qquad \sigma''(\omega) = -\frac{d}{S} \cdot \frac{Z''}{|\hat{Z}|^2}. \qquad (2.5)$$

From the definition of electric power for a complex impedance [9], it can be easily concluded that the real part of conductivity describes the dissipative aspect of ion dynamic, whereas the conservative aspect of ion dynamic is associated with the imaginary part.

2.2 *Conductivity spectra of RC circuits*

The electrical response of ionic electrolytes is typically analyzed by comparing them to equivalent circuits. A basic equivalent circuit consists of two parallel RC (resistor-capacitor) circuits connected in series. The first circuit represents the bulk properties of the electrolyte, while the second models the electrode-electrolyte interfaces [5].

Due to the similarities between parallel RC circuits and ionic electrolytes placed between two metallic electrodes [10], studying the conductivity behavior of these circuits provides valuable insights into the electrical response of ionic conductors. This approach aids in understanding and analyzing the complex behavior of these materials.

In this section, we will examine the spectra of the real part of conductivity for two distinct circuits. This analysis will shed light on the characteristic responses of ionic electrolytes under various conditions.

The first case is the parallel connection of an electrical resistance R and a capacitor C (Figure 1). The impedance of this circuit is given by

$$\frac{1}{Z} = \frac{1}{R} + i\omega \cdot C \qquad (2.6)$$

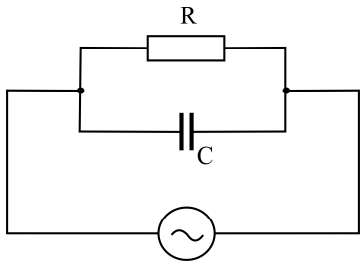

Figure 1. Parallel RC circuit

Equations (2.5) and (2.6) yield the real and imaginary parts of conductivity as

$$\sigma' = \frac{d}{R \cdot S} \quad ; \qquad \sigma'' = \omega \cdot C \cdot \frac{d}{S} \qquad (2.7)$$

These equations reveal that the real part of the conductivity is independent of the frequency. As a result, the conductivity spectrum in this case should appear as a straight horizontal line.

The second case considers a serial connection of two parallel RC circuits, which is depicted in (Figure 2). The impedance of this circuit can be expressed as

$$\hat{Z}_{tot} = Z'_{tot} + iZ''_{tot},$$

with

$$Z'_{tot} = Z'_1 + Z'_2 = \frac{R_1}{1+(\omega R_1 C_1)^2} + \frac{R_2}{1+(\omega R_2 C_2)^2}, \tag{2.8}$$

and

$$Z''_{tot} = Z''_1 + Z''_2 = -\frac{(\omega R_1 C_1)\cdot R_1}{1+(\omega R_1 C_1)^2} - \frac{(\omega R_2 C_2)\cdot R_2}{1+(\omega R_2 C_2)^2}. \tag{2.9}$$

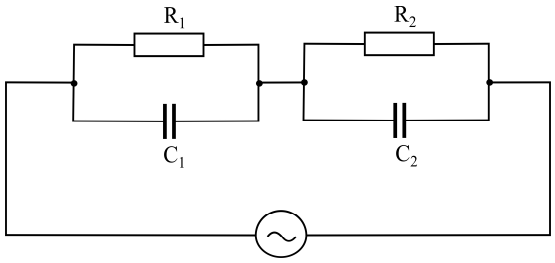

Figure 2. Serial connection of two parallel RC circuits

Substitution of the real and imaginary parts of impedance in equation (2.5) yields the following statement for the real part of the conductivity

$$\sigma'_{tot} = \frac{(R_1+R_2)+\left[R_1(\omega R_2 C_2)^2 + R_2(\omega R_1 C_1)^2\right]}{(R_1+R_2)^2+\left[R_1(\omega R_2 C_2)+R_2(\omega R_1 C_1)\right]^2}\cdot\frac{d}{S}. \tag{2.10}$$

Where $d = d_1 + d_2$, is the sum of the thicknesses of two capacitors. The areas of the capacitors are supposed to be equal $S = S_1 = S_2$. In this case, the total conductivity is frequency dependent, and at low frequencies it becomes

$$\omega \to 0 \Rightarrow \sigma'_{tot} = \frac{1}{R_1+R_2}\cdot\frac{d}{S}, \tag{2.11}$$

which is independent of frequency but depends on the resistances. At high frequencies, the conductivity becomes a constant value again

$$\omega \to \infty \Rightarrow \sigma'_{tot} = \frac{(R_1C_1^2 + R_2C_2^2)}{(C_1+C_2)^2\cdot R_1\cdot R_2}\cdot\frac{d}{S}, \tag{2.12}$$

For $R_2 >> R_1$ and $C_2 >> C1$, it results in

$$\sigma'_{tot} = \frac{1}{R_1}\cdot\frac{d}{S}. \tag{2.13}$$

In ionic conductors, R_1 and C_1 typically represent bulk properties, while R_2 and C_2 describe interface properties. For a blocking electrode, the conditions $R_2 >> R_1$ and $C_2 >> C_1$ are generally satisfied. In ionic materials with blocking electrodes, ions cannot transfer between the electrolyte and electrodes, effectively making R_2 infinite. The electrode-electrolyte interface is usually much thinner than the electrolyte itself, resulting in a significantly higher interfacial capacitance compared to the bulk electrolyte capacitance.

Figure 3 illustrates the conductivity spectra of these circuits. The conductivities are calculated using equations (2.7) and (2.10), with the parameters specified in the figure, over a frequency range of 10^{-3} Hz to 10^{3} Hz. The solid line represents the case of a serial connection of two parallel RC circuits (σ_{tot}). In this configuration, there exists a frequency range where the conductivity becomes frequency-dependent. The position and shape of this frequency-dependent region are determined by the parameters stated in Figure 3, in accordance with equation (2.10). The parameters shown in Figure 3 have been chosen in such a way that they are consistent with the above descriptions regarding the bulk and interface characteristics. At high frequencies, the total conductivity approaches σ_1, while at low frequencies, it stabilizes at a constant value between σ_1 and σ_2.

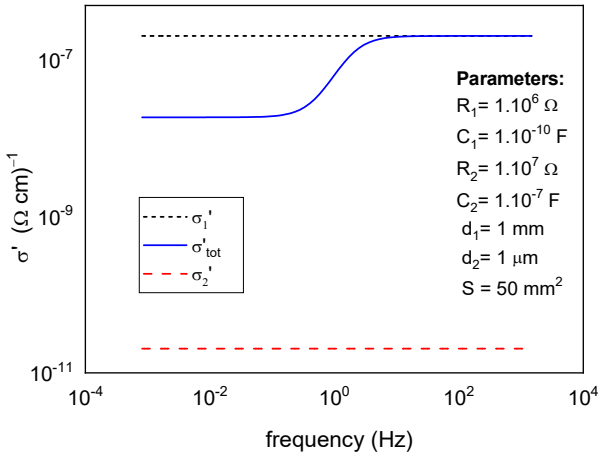

Figure 3. Conductivity spectra for σ'_1 (parallel R_1C_1) and σ'_2 (parallel R_2C_2), and for σ'_{tot} a serial connection of two parallel RC circuits

2.3 *Impedance semicircles*

The impedance of an electric circuit containing an electrical resistance R and a capacitor C, in the case of parallel connection (Figure 1), can be derived from:

$$\frac{1}{\hat{Z}} = \frac{1}{R} + i\omega \cdot C \qquad (2.14)$$

The real and imaginary parts of impedance can be written as

$$Z' = \frac{R}{1+(\omega RC)^2} \quad ; \qquad Z'' = -\frac{\omega R^2 C}{1+(\omega RC)^2} . \qquad (2.15)$$

The angular frequency ω connects the real and imaginary parts of impedance. A plot of the imaginary part of impedance (-Z") versus the real part (Z') in the complex plane results in a semicircle with a diameter equal to the resistance R. This representation is known as a Nyquist plot or Cole-Cole plot [11]. Figure 4 illustrates an example of such an impedance semicircle. Key features include: The arrow indicates the direction of increasing frequency. The angular frequency at the semicircle's maximum point is defined as ω_p. At this point, the real part of the impedance equals its imaginary part, leading to the following relationship

$$C = \frac{1}{R\omega_p} \qquad (2.16)$$

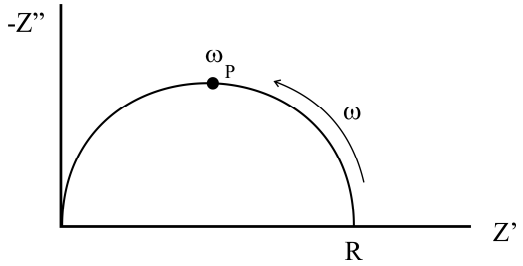

Figure 4. Impedance semicircle

The impedance spectrum for the serial connection of two parallel RC circuits (Figure 2) is shown in Figure 5. It is assumed that the resistance values R_1 and R_2, as well as the capacitance values C_1 and C_2, are all distinct from one another.

The impedance spectrum exhibits two distinct semicircles, which are obtained by numerically solving for the real (Z') and imaginary (Z") components of the impedance over a frequency range of 1 Hz to 10^8 Hz. The diameters of the individual semicircles correspond directly to the values of the respective resistance parameters, R_1 and R_2.

By applying Equation (2.16) to each of the semicircles separately, the individual capacitance values C_1 and C_2 can be reproduced from the impedance spectrum.

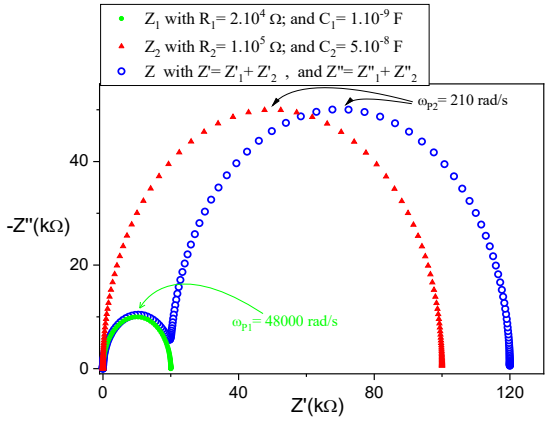

Figure 5. Impedance semicircles for serial combination of two parallel RC circuits

For $R_1 = R_2$ and $C_1 = C_2$, the impedance response results in only one semicircle with diameter $R = R_1 + R_2$, and capacity $C = C_1/2 = C_2/2$, this case is shown in Figure 6.

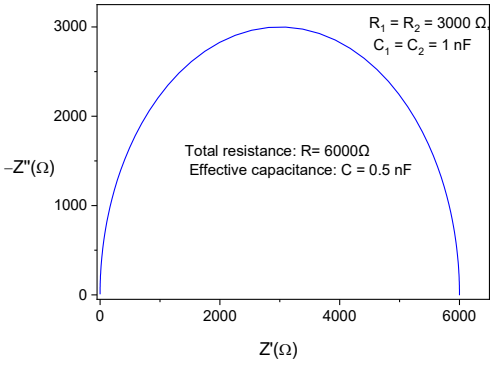

Figure 6. Simulated impedance response for a series combination of two parallel RC circuits, for $R_1 = R_2$ and $C_1 = C_2$

Under the conditions where $R_1 = R_2$, but $C_1 \neq C_2$, the impedance spectrum will exhibit two partially overlapping semicircles. The degree of overlap between the two semicircles depends on the difference between the capacitance values C_1 and C_2. An example of this scenario is illustrated in Figure 7. As the difference between C_1 and C_2 decreases, the overlap region between the two semicircles becomes more prominent. The maximum overlap occurs when $C_1 = C_2$. In this special case, the impedance spectrum simplifies to a single, well-defined semicircle, as shown in Figure 6.

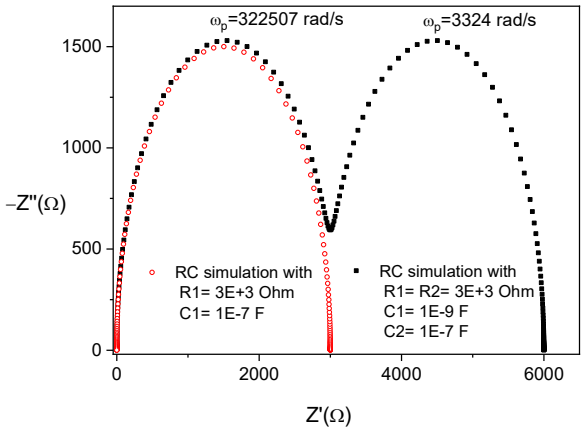

Figure 7. Simulation of impedance semicircle for the circuit shown in the Fig with $R_1 = R_2 = 3000\ \Omega$, and $C_1 = 1$ nF and $C_2 = 100$ nF. The resulted resistances and capacitances from these semicircles are the same as the supposed values.

2.4 *Equivalent circuit for ionic conductors*

The impedance semicircles observed in AC measurements can be modeled using equivalent circuits. A schematic diagram of a sample is shown in Figure 8-a. In this diagram, the glass layer sandwiched between two metallic electrodes can be represented as a capacitor, C_{vol}. The glass layer acts as a dielectric material in this capacitive element. Additionally, the glass layer contains mobile lithium ions, which contribute a limited electrical resistance, R_{vol}. This resistance is in parallel with the capacitive element, as the ions can provide a conductive pathway through the glass.

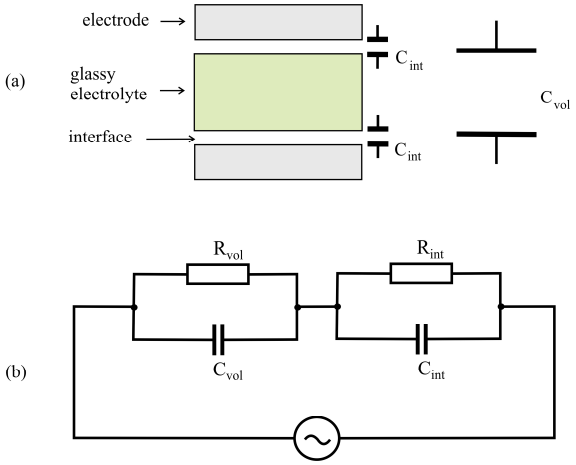

Figure 8. (a) Schematic diagram of a glassy ionic electrolyte between two metallic electrodes. The interfaces, due to the polarization effect, can be considered as capacitors. **(b)** Equivalent circuit corresponds to the described sample.

Application of an electric field between electrodes induces ion polarization in both the glass layer and at the interfaces. Each glass-electrode interface forms a capacitor, denoted as C_{int}. For non-blocking electrodes, ionic transport across these interfaces is possible, resulting in a finite resistance. Consequently, each interface can be modeled as a parallel RC circuit.

Due to symmetry, it's reasonable to assume that both interfaces have identical geometrical shapes and structural properties. Therefore, their equivalent circuit can be represented by two identical parallel RC circuits. As discussed in section 2.2, two identical parallel RC circuits produce a single semicircle in the impedance spectrum. Thus, the appropriate equivalent circuit for these samples consists of one parallel RC circuit for the glass volume and another for both interfaces combined (Figure 8.b).

Impedance spectroscopy measurements are typically conducted over a specific frequency range. A wide frequency range would reveal all parts of the semicircles, as shown in Figures 5-7. However, the required frequency range depends on the material's electrical properties, such as equivalent resistivity and capacitance, and is limited by the capabilities of impedance measurement devices. This limitation is particularly significant when two semicircles are expected, but only portions may be visible within the available frequency range.

Figure 9 illustrates how the observable parts of the semicircles depend on the sample's electrical properties within a limited frequency range. This is demonstrated through simulations of impedance semicircles for the equivalent circuit in Figure 8.b, with parameters presented in Table 1. Both simulations in Figures 9a and 9b use an identical frequency range but represent samples with the same interface properties and different volume properties. The frequency at the onset of the second semicircle is denoted by ν_{12}, which depends on both volume and interface equivalent elements. For the sample with higher volume resistivity, ν_{12} is lower, resulting in a smaller visible arc of the second semicircle.

Table 1. Overview of the parameters for the semicircle simulation in Figure 9

Figure	$R_{vol}(\Omega)$	$C_{vol}(F)$	$R_{int}(\Omega)$	$C_{int}(F)$	frequency range (Hz)
9a	400	$1 \cdot 10^{-8}$	$4 \cdot 10^{5}$	$1 \cdot 10^{-7}$	50 - $2 \cdot 10^{6}$
9b	8000	$2 \cdot 10^{-9}$	$4 \cdot 10^{5}$	$1 \cdot 10^{-7}$	50 - $2 \cdot 10^{6}$

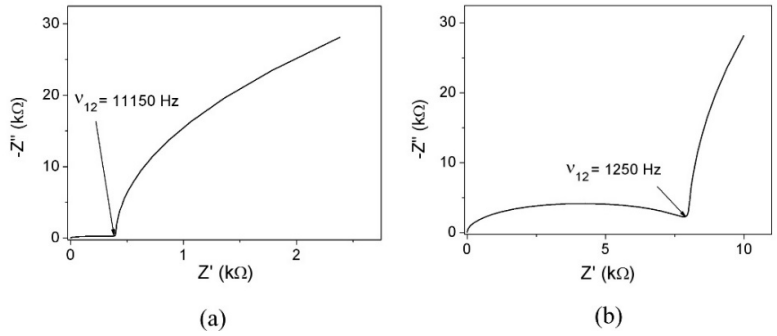

Figure 9. Simulated impedance spectra for two samples with identical interfacial properties but differing bulk characteristics

2.5 *Equivalent circuit for ionic conductors*

The experimental results shown in this research were obtained using an impedance analyzer. It provides frequencies between 5'Hz- 13'MHz with a frequency resolution of 1'mHz to 1 Hz, depending on the frequency range. Oscillator amplitude ranges from Vrms= 5'mV to 1.1V. Real and imaginary parts of impedance as a

function of frequency are measured automatically by the analyzer. The temperature of the sample is measured by a Eurotherm temperature controller. A PC is used to control both the analyzer and the temperature controller. When the temperature reaches the desired value, electrical measurements are performed automatically.

Figure 10 displays the impedance semicircle of a bulk lithium borate (0.20 $Li_2O\cdot$ 0.80 B_2O_3) sample. The absence of a second semicircle is due to the low-frequency limitations of the measurement device. Closer examination reveals that this impedance graph does not represent a perfect semicircle, as its height is less than half its diameter. Consequently, the data points cannot be accurately fitted by a simple semicircle model.

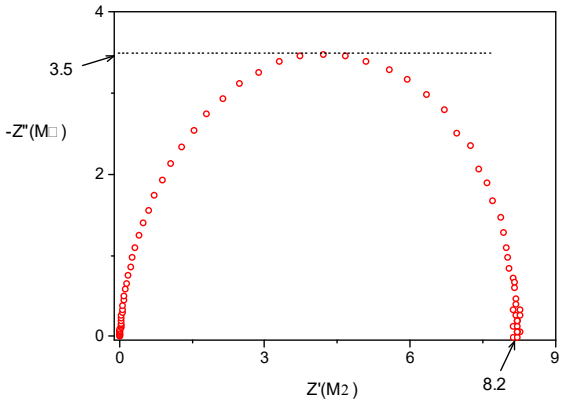

Figure 10. Impedance complex plain plot of a bulk 0.20 $Li_2O\cdot$ 0.80 B_2O_3 glass with a thickness of 0.82 mm at 220°C

This deviation indicates that a parallel RC circuit is not an ideal equivalent circuit for this system. A more appropriate alternative is the "Constant Phase Element" (CPE), which replaces the capacitor [12]. The impedance of the CPE is defined by an empirical function:

$$\frac{1}{\hat{Z}_{CPE}} = Q\cdot(i\omega)^n, \qquad (2.17)$$

Where Q is the numerical value of the admittance at ω = 1 rad/s. n is a constant between 0 and 1, determining the degree of deviation from an exact semicircle. When n = 1, equation (2.17) yields the impedance of a capacitor, with Q = C.

Typically, measured impedance spectra are well-described by R-CPE circuits. Therefore, the equivalent circuit should be modified as shown in Figure 11, where the CPE is represented by the symbol ⫽↗.

Figure 12 compares two different fitting models: R-C and R-CPE. This comparison clearly demonstrates that the R-C fitting is inadequate for this case, while the R-CPE model provides a superior fit to the experimental data.

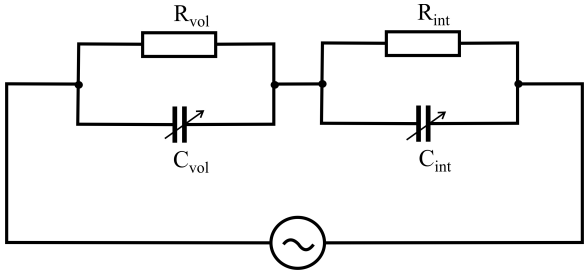

Figure 11. Enhanced equivalent circuit model incorporating Constant Phase Elements (CPEs) for the sample described in Figure 8

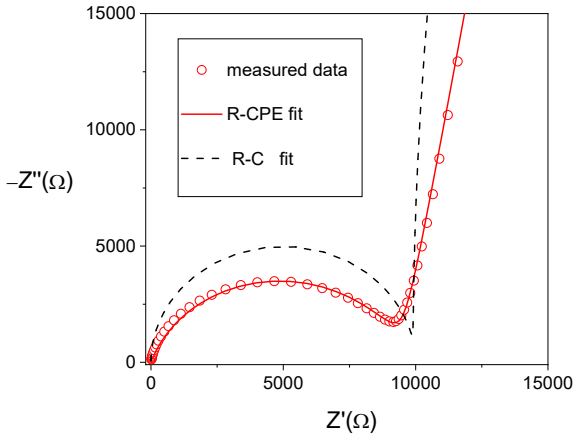

Figure 12. Impedance diagram of a 0.20 Li_2O· 0.80 B_2O_3 glass thin film with a thickness of 360 nm at 180 °C. Dashed and solid lines show the fitted data based on RC and RCPE models, respectively

The impedance of a parallel R-CPE circuit is expressed as

$$\frac{1}{\hat{Z}} = \frac{1}{R} + \frac{1}{\hat{Z}_{CPE}} \qquad (2.18)$$

Insertion of definition (2.17) in equation (2.18) for real and imaginary parts of impedance yields

$$Z' = \frac{R\left(1 + RQ\omega^n \cos\frac{n\pi}{2}\right)}{1 + 2RQ\omega^n \cos\frac{n\pi}{2} + \left(RQ\omega^n\right)^2} \qquad (2.19)$$

and

$$Z'' = -\frac{R^2 Q\omega^n \sin\frac{n\pi}{2}}{1 + 2RQ\omega^n \cos\frac{n\pi}{2} + \left(RQ\omega^n\right)^2}. \qquad (2.20)$$

The conductivity can be derived by substituting equations (2.19) and (2.20) into equation (2.5). When n is close to one, the CPE behaves similarly to a capacitive element, with the CPE parameter Q representing a capacity C. The frequency at which |Z''| reaches its maximum, ωp, is found by using the first derivative of equation (2.20)

$$\omega_p = \frac{1}{(RQ)^{\frac{1}{n}}}. \qquad (2.21)$$

If we assume that ωp for a parallel R-CPE circuit is equivalent to ωp for a parallel R-C circuit, as is often done [13], comparing equations (2.16) and (2.21) yields

$$C = R^{\frac{1-n}{n}} \cdot Q^{\frac{1}{n}}. \qquad (2.22)$$

However, equation (2.21) clearly shows that ω_p of the CPE depends on the parameter n. Thus, the assumption of equality between ω_p for R-CPE ($n \neq 1$) and R-C ($n = 1$) is not strictly correct. Nevertheless, equation (2.22) may still serve as a good approximation when either n or the product of RQ is close to one.

To establish a more accurate relationship between Q and C such that $\omega_p = \omega'_p$, we consider the impedance diagram of R-CPE as part of a semicircle of R-C, as illustrated in Figure 13.b. In this case, the ω_p of the two

impedance diagrams coincide exactly. In the figure, R and R' denote the resistances of the R-CPE circuit and its corresponding RC circuit, respectively. Using the geometry of the semicircles, the relationship between these two resistances can be expressed as:

$$\frac{R'}{2} = \frac{\frac{R}{2}}{\cos\left((1-n)\cdot\frac{\pi}{2}\right)}. \qquad (2.23)$$

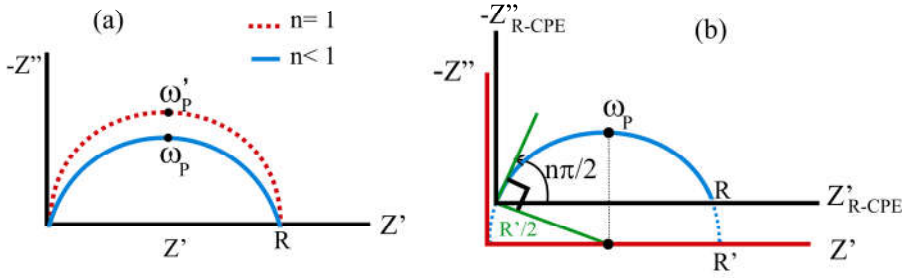

Figure 13. Conversion of CPE parameter Q into C. (a) Comparison of two semicircles with different n and different ω_p. (b) The R-CPE impedance graph with n<1 (solid line) is regarded as a part of a semicircle with n=1 (pointed line).

Inserting this relation into equation (2.16), and considering the equality of $\cos\left((1-n)\cdot\frac{\pi}{2}\right)$ and $\sin\left(n\cdot\frac{\pi}{2}\right)$, yields the value of ω_p for the R-C circuit as

$$\omega_p = \frac{\sin\left(n\cdot\frac{\pi}{2}\right)}{RC}. \qquad (2.24)$$

Combining equations (2.21) and (2.24) results in

$$C = R^{\frac{1-n}{n}}\cdot Q^{\frac{1}{n}}\cdot\sin\left(n\cdot\frac{\pi}{2}\right). \qquad (2.25)$$

At first glance, deriving this relation by comparing an RC circuit with an R'-CPE circuit (where $R \neq R'$) might seem as problematic as relation (2.22). Indeed, directly comparing RC and R-CPE circuits is not strictly correct due to their different physical properties.

As expected, this relation reduces to equation (2.22) when n = 1. For n = 0.7, the capacity calculated using equation (2.25) is approximately 11% smaller than that obtained from equation (2.22).

2.6 *Conductivity spectra of lithium borate glasses*

Figure 3 demonstrated that for a series connection of two parallel RC circuits, the conductivity is frequency-dependent, and this frequency dependence varies across different frequency ranges. Considering this, in this section, we will study the experimental results obtained from the conductivity spectra of lithium borate in various frequency regions.

Figure 14 presents the measured conductivity spectra for a 0.20 Li_2O · 0.80 B_2O_3 sample as a function of frequency at various temperatures ranging from 185°C to 330°C. These spectra were recorded over a frequency range of 5 Hz to 2 MHz. As temperature increases, the conductivity enhances due to increased ion mobility.

Unlike the conductivity of a single RC circuit, the measured conductivity exhibits frequency-dependent behavior. At a constant temperature, the conductivity graph can be divided into two regions: low and high frequencies.

At low frequencies, the specific conductivity remains independent of frequency and is referred to as the 'dc conductivity' (σ_{dc}). σ_{dc} results from long-range ion transport. According to K. Funke's 'jump relaxation model' [14], long-range ion transport involves successful jumps of ions, in contrast to the back-and-forth jumps between equilibrium positions.

At higher frequencies, the conductivity is no longer constant but increases monotonically with frequency. This frequency dependence arises from the forward-backward jumps of ions, which are only detectable at small time scales (high frequencies).

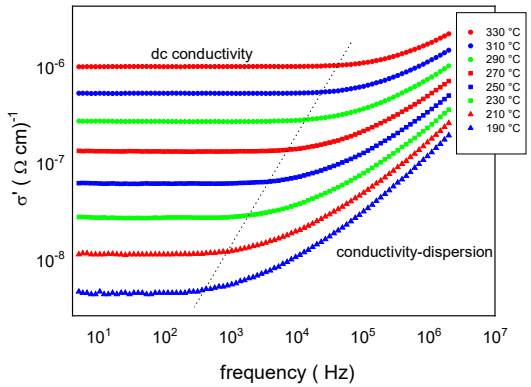

Figure 14. Frequency-dependent conductivity spectra of 0.20 Li_2O· 0.80 B_2O_3 bulk glass for different Tempretures

In an ion conductor with higher conductivity (0.35 Li_2O · 0.65 B_2O_3), there are more mobile ions, resulting in higher dc conductivity. It also becomes possible to observe the double layer conductivity within the same frequency range when the lowest frequency is limited to 5 Hz (Figure 15).

The double layer conductivity (between the glass layer and metallic electrodes), visible in the spectra at low frequencies, can be explained by the jump relaxation model, similar to the bulk glass conductivity. At very low frequencies, for non-blocked electrodes, we expect interfacial ion transport between the glass layer and electrode. This ion transport conductivity is frequency-independent in this range and usually much lower than the dc conductivity of the glass film.

At slightly higher frequencies, the forward-backward jumping of ions between the glass layer and the electrode becomes measurable, causing the interfacial conductivity to increase with frequency. The transition frequencies depend on both measurement temperature and interface structure. Interfacial conductivity becomes visible only in certain frequency ranges, depending on conductivity values, which is why it's not observed in Figure 14.

Figure 15 shows the conductivity spectra of a 0.35 Li_2O · 0.65 B_2O_3 sample with a thickness of 0.45 mm. Three distinct areas, corresponding to different conductivity mechanisms, are visible:

The area between two dashed lines represents the dc conductivity of the glass, arising from long-range ion transport. Here, conductivity is frequency-independent and only temperature-dependent.

The high-frequency area (right of the dashed line) can be explained by forward-backward jumps of ions in the glass volume, as previously mentioned.

The low-frequency area, new compared to Figure 14, shows behavior similar to the high-frequency area but with lower conductivity. This is attributed to the glass-electrode interface, caused by forward-backward jumping of ions between glass and electrodes. Either the conductivity is insufficient, or the frequency is still too high to record the interfacial ionic conductivity.

Sputtered glassy thin films show measurable ionic motion at the glass-electrode interface at high temperatures. Figure 16 displays the conductivity spectra of a thin glass film of 0.25 Li_2O · 0.75 B_2O_3 with a thickness of 230 nm.

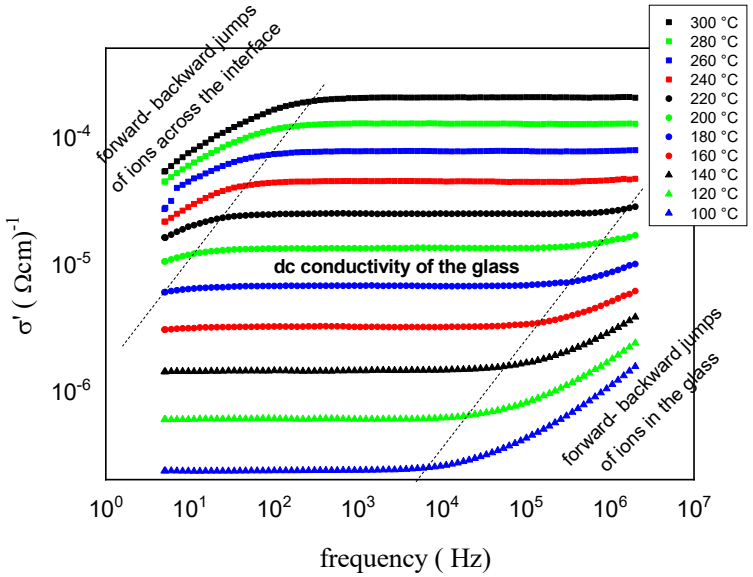

Figure 15. Conductivity spectra of 0.35 Li_2O· 0.65 B_2O_3 bulk glass with a thickness of 0.45 mm, measured at various temperatures.

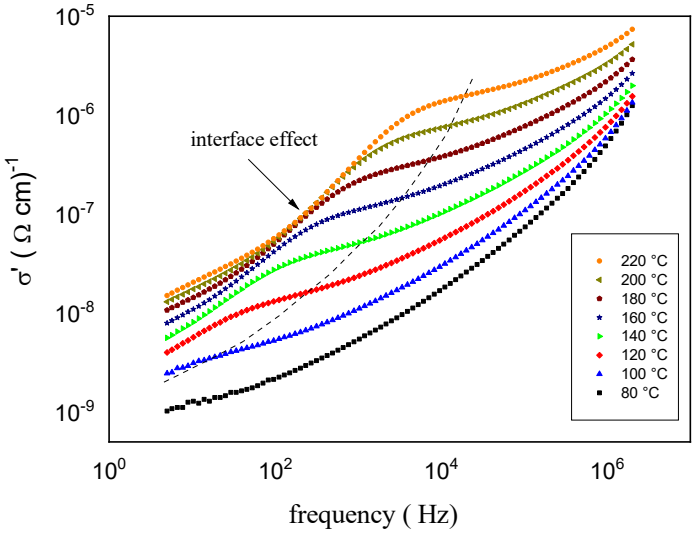

Figure 16. Conductivity spectra of a 0.25 Li_2O· 0.75 B_2O_3 glass film with a thickness of 230 nm. The spectra are taken at different temperatures and over a frequency range of 5Hz to 2MHz.

To analyze the conductivity behavior of thin films, we focus on a selected spectrum recorded at 220 °C. Figure 17 illustrates four distinct conductivity regimes in this spectrum, which can be described as follows:

Part 1, Glass Film Conductivity: This regime is characterized primarily by the forward-backward jumps of ions within the glass film. The conductivity in this area exhibits a clear frequency dependence.

Part 2, DC Conductivity of the Glass Film: Compared to the dc conductivity of bulk glasses (as shown in Figures 14 & 15), the dc conductivity of the thin glass film appears to have a slight frequency dependence. This phenomenon can be attributed to two factors: a) The small difference between the conductivities of the glass film and the interfaces results in less distinct boundaries between different areas, unlike in bulk glasses. b) An overlap occurs between the dc conductivity and the frequency-dependent conductivities on both sides, causing the conductivity in this region to show some frequency dependence. To quantify the dc conductivity, we consider the point of inflection, which yields a conductivity value of approximately 1.7×10^{-6} $(\Omega\ cm)^{-1}$.

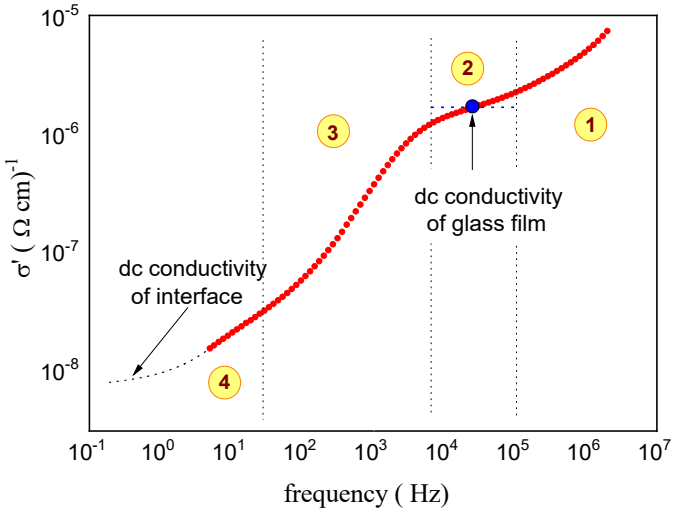

Figure 17. Conductivity spectrum of a thin film glass of 0.25 $Li_2O\cdot$ 0.75 B_2O_3 at 220 °C with a thickness of 230 nm

Part 3, Interface Conductivity between Glass Film and Electrodes: The interface conductivity arises from two distinct contributions. Forward-backward ion motions across the glass-electrode interface, and electrical interaction of two parallel RC circuits.

Part 4, Low-Frequency Conductivity Analysis: The measured data points in this region represent a combination of the interface dc conductivity and the conductivity described in Part 3. Extrapolation to lower frequencies is expected to reveal the pure dc conductivity, as indicated by the dashed line. Key observations include:

- Estimated dc conductivity: Approximately 7.7×10^{-9} $(\Omega\ cm)^{-1}$
- Comparison to glass film: This value is 220 times smaller than the dc conductivity of the glass film
- Composition: The predicted dc conductivity in this region is a composite of two dc conductivities: a. Glass dc conductivity b. Interface dc conductivity (Refer to equation (2.11) and Figure 3 for details)
- Interfacial dominance: If the interface conductivity is significantly lower than that of the glass, the conductivity in this region can be approximated as the interfacial dc conductivity

4. Conclusions

Our comprehensive study of ionic conductors using impedance spectroscopy has revealed several key insights:

1. The conductivity spectra of ionic conductors exhibit complex frequency-dependent behavior, with distinct regimes corresponding to bulk, interfacial, and electrode processes.
2. Thin film samples show unique characteristics compared to bulk materials, particularly in the visibility and interpretation of interfacial effects.
3. The Constant Phase Element (CPE) proves to be a crucial tool for accurately modeling the non-ideal behavior observed in real ionic conducting systems, overcoming the limitations of simple RC circuit models.
4. We have derived and validated a new relationship (equation (2.25)) between CPE parameters and conventional capacitance, providing a more accurate method for interpreting impedance data.
5. The study highlights the importance of considering frequency range limitations in impedance measurements and their impact on data interpretation, especially when multiple relaxation processes are present.

These findings contribute to an improved understanding of ion transport mechanisms in glassy electrolytes and offer practical guidelines for analyzing impedance spectroscopy data. The insights gained from this work have implications for the development and optimization of ionic conductors for various applications, including solid-state batteries and sensors.

Future work should focus on extending these analyses to a broader range of compositions and structures, as well as developing more sophisticated models to account for the complex interplay between bulk and interfacial processes in ionic conducting systems. Additionally, the application of these findings to the design of improved electrolyte materials for specific technological applications presents an exciting avenue for further research.

Conflicts of Interest

The author declares that there are no conflicts of interest regarding this article.

References

1. Kim JG, Son B, Mukherjee S, Schuppert N, Bates A, Kwon O, Choi MJ, Chung HY, Park S. A review of lithium and non-lithium based solid state batteries. *J. Power Sources* 2015, 282:299-322.
2. Bates AM, Preger Y, Torres-Castro L, Harrison KL, Harris SJ, Hewson J. Are solid-state batteries safer than lithium-ion batteries? *Joule* 2022, 6(4):742-755.
3. Deroco PB, de Fátima Giarola J, Júnior DW, Lorga GA, Kubota LT. Based electrochemical sensing devices. In: Comprehensive analytical chemistry. 2020, Vol 89, Amsterdam: Elsevier, pp. 91-137.
4. Zheng F, Kotobuki M, Song S, Lai MO, Lu L. Review on solid electrolytes for all-solid-state lithium-ion batteries. *J. Power Sources* 2018, 389, 198-213.
5. Irvine JTS, Sinclair DC, West AR. Electroceramics: Characterization by Impedance Spectroscopy. *Adv. Mater.* 1990, 2(3): 132-138.
6. Orazem ME, Tribollet B. Electrochemical Impedance spectroscopy. 2017, Hoboken: Wiley.
7. Barsoukov E, Macdonald JR. Impedance spectroscopy. 2005, Hoboken: Wiley.

8. Ivers-TIFFÉE E, Weber A. Evaluation of electrochemical impedance spectra by the distribution of relaxation times. *J. Ceram. Soc. Jpn.* 2017, 125(4): 193-201.
9. Reitz JR. Foundations of electromagnetic theory. 2009, Hoboken: Pearson Education India.
10. Macdonald JR. Impedance spectroscopy. *Ann. Biomed. Eng.* 1992, 20: 289-305.
11. Mei B, Munteshari O, Lau J, Dunn B, Pilon L. Physical interpretations of Nyquist plots for EDLC electrodes and devices. *J. Phys. Chem. C* 2017, 122(1): 194-206.
12. Souquet JL. Ionic transport in amorphous solid electrolytes. *Annu. Rev. Mater. Sci.* 1981, 11(1): 211-231.
13. Hsu CH, Mansfeld, F. Technical Note: Concerning the conversion of the constant phase element parameter Y0 into a capacitance. *Corrosion* 2001, 57(9): 747-748.
14. Funke K. Jump relaxation in solid electrolytes. *Prog. Solid State Chem.* 1993, 22(2): 111-195.

How to cite this article: Shoar Abouzari MR. Comprehensive Analysis of Impedance Spectroscopy and Conductivity Evaluation of Ionic Transport in Lithium Borate Glasses. *Curr. Appl. Sci.*, 2024, 2(2):119-134. https://doi.org/10.22034/cas.2024.476900.1042